Band alignment issues related to HfO2/SiO2/p-Si gate stacks

S. Sayan, T. Emge, E. Garfunkel, Xinyuan Zhao, L. Wielunski et al.

Citation: J. Appl. Phys. 96, 7485 (2004); doi: 10.1063/1.1803107
View online: http://dx.doi.org/10.1063/1.1803107
View Table of Contents: http://jap.aip.org/resource/1/JAPIAU/v96/i12
Published by the American Institute of Physics.

Band alignment issues related to $HfO_2/SiO_2/p$-Si gate stacks

S. Sayan, T. Emge, and E. Garfunkel[a)]
Department of Chemistry, Rutgers University, Piscataway, New Jersey 08854

Xinyuan Zhao, L. Wielunski, R. A. Bartynski, and David Vanderbilt
Department of Physics and Astronomy, Rutgers University, Piscataway, New Jersey 08854

J. S. Suehle
Semiconductor Electronics Division, National Institute of Standards and Technology, Gaithersburg, Maryland 20899

S. Suzer
Department of Chemistry, Bilkent University, 06533 Ankara, Turkey

M. Banaszak-Holl
Department of Chemistry, University of Michigan, Ann Arbor, Michigan 48109

(Received 12 February 2004; accepted 4 August 2004)

The valence and conduction band densities of states for the $HfO_2/SiO_2/Si$ structure are determined by soft x-ray photoemission and inverse photoemission. First principles calculations are used to help in assigning valence band maxima and conduction band minima. The energies of defect states at the band edges are estimated by comparing the theoretical and experimental results. Determinations of the local surface potentials before and after a forming gas anneal are used to help determine the possible location of the charge in the film. © *2004 American Institute of Physics*.
[DOI: 10.1063/1.1803107]

I. INTRODUCTION

The need for a high permittivity (high-*k*) material for future nanoelectronic devices is clear.[1] To replace SiO_2 with a high-*k* dielectric, one of many requirements is that both valence and conduction band offsets of the material (with respect to the silicon band edges) need to be greater than 1 eV.[2] Although many reports of high-*k*/silicon gate stack structures have appeared, most of which explore HfO_2 and ZrO_2 based materials, a consensus on the best dielectric material has yet to be reached.

Recently we have reported that the electronic structures (including energy gap, band offsets, charge neutrality level, and permittivity…) of these materials are strongly phase (crystal structure) dependent.[3,4,28] Thus the crystal structure of this class of high-*k* dielectrics should be reported along with any experimental data if a valid comparison of results from different experimental techniques is desired. In this study, we examine HfO_2 deposited on SiO_xN_y/p-Si by photoemission spectroscopy (PES) and inverse photoemission spectroscopy (IPES). The experimental determination of valence band maxima (VBM) and conduction band minima (CBM) remains a controversial issue. The reports of high-*k* materials on silicon using photoemission and optical methods usually employ a "straight-line" method where the valence and conduction edges are determined using a linear extrapolation of the data to the "background" intensity level. Although this particular method does not have a strong physical justification (the band shape is part of the intrinsic nature of the material and is rarely "straight"), it serves as a common method for all in the field to compare their work. In general, polycrystalline semiconductors present a higher concentration of defects and imperfections than bulk single crystals. The presence of structural disorder can also be related to deviations from ideal stoichiometry and/or impurities. One major consequence is that new electronic states may appear which manifest themselves as increased densities of states in the vicinity of the band edges; these are sometimes called band tail states.[5] The presence of band tail states not only reduces the observed gap but it may increase carrier transport across or scattering in (or near) the dielectric. The defect bands may also overlap with the bands of the perfect crystal.[6] The experimentally observed density of states (DOS) can be considered as a superposition of the perfect crystal DOS and defect bands. A change in the band edge would change the offset assignments and lead to a reduced "effective gap." The exact value of an intrinsic energy gap has yet to be determined for an ultrathin crystalline dielectric film since all high-*k* films reported to date are either polycrystalline or amorphous and have crystal imperfections (defects) which inevitably contribute to the electronic properties. What are needed are careful measurements of bulk single crystals and crystalline ultrathin films to confirm theoretical predictions, a goal yet to be realized for this class of oxides.

Electronic states can appear either near the edges or closer to midgap that can be either structural or compositional in nature (e.g., metal or oxygen vacancy).[7] The charge neutrality level (CNL) of these states with respect to the Fermi energy will determine their occupancy and charge, as well as their effect on the band alignment. The rate at which the occupancy of these states change as the electrode voltages are varied, will depend on their distance from the electrode and other defects, as well as their energy, and may be critical in determining device electrical characteristics.

[a)]Electronic mail: garf@rutchem.rutgers.edu

II. EXPERIMENT

HfO_2 films were deposited on 11 Å SiO_xN_y/p-Si at ~400 °C using chemical vapor deposition, with Hf-tetra-tert-butoxide as the precursor; details of the growth can be found elsewhere.[8] The primary substrate used in the studies reported here was *p*-type Si(100) with a doping concentration of $\sim 1\times10^{15}$ cm^{-3}. The thickness of the SiO_xN_y film was 11 Å as measured by medium energy ion scattering (MEIS), and the O:N ratio in the oxynitride was ~4:1. By MEIS, the stoichiometry of the as-deposited overlayer was determined to be $HfO_{2.17\pm0.06}$. The work reported in this paper used HfO_2 films of 10–30 Å and up to 1000 Å for x-ray diffraction (XRD) measurements. The forming gas anneals were done at 400 °C and 1 Torr forming gas pressure (5% H_2/Ar). Soft x-ray photoemission measurements were performed at Brookhaven National Laboratories on the U8B beamline using 120–400 eV photon energies. The inverse photoemission studies were performed in fluorescence mode in the 18–22 eV electron energy range at Rutgers University. The x-ray photoelectron spectroscopy measurements were performed on a Kratos XSAM 800 utilizing Mg $K\alpha$ (1253.6 eV) as the excitation photon energy.

Rutherford backscattering spectroscopy (RBS) measurements are done using a 2 MeV He^{++} beam. The wide-angle x-ray scattering patterns of several samples of HfO_2 thin layers on Si substrates were obtained using a Bruker HiStar area detector and an Enraf-Nonius FR571 rotating anode x-ray generator equipped with a graphite monochromator (Cu $K\alpha$; $\lambda = 1.5418$ Å) operating at 40 kV and 50 mA. The sample to detector distance was 5.5 cm and the standard spatial calibration was performed at that distance. Scans were 3 deg wide in omega (ω) with fixed detector, or Bragg, angle (2θ) of 40 deg, and fixed platform (ϕ and χ) angles of 0 and 0 deg, respectively. In all cases, the count rate for the area detector did not exceed 100 000 cps.

III. RESULTS AND DISCUSSION

A. PES and IPES measurements

Figure 1 shows the photoemission spectra and peak assignments in the valence band region for a 28 Å $HfO_2/SiO_xN_y/p$-Si gate stack. The intense feature in the 17–20 eV region is the Hf 4*f* spin-orbit doublet. The curve fitting was performed after a Shirley background subtraction. A pair of Gaussians was used to model this region representing the spin-orbit splitting of the 4*f* level. The spin-orbit splitting was found to be 1.66 eV. The intensity ratio was ~4:3, in agreement with the expected theoretical ratio. The binding energies of the $4f_{7/2}$ and $4f_{5/2}$ peaks were 17.65 and 19.31 eV, respectively.

The photoemission and inverse photoemission data obtained from a 28 Å $HfO_2/SiO_xN_y/p$-Si are shown in Fig. 2. The valence band mainly consists of O 2*p* like nonbonding orbitals of π symmetry while the conduction band is mainly Hf 5*d* like nonbonding orbitals. All energies are referenced to the Fermi level which is determined by a clean polycrystalline gold or platinum sample. Special care is taken when determining the spectrometer response functions for both IPES and PES. This is accomplished by modeling the region

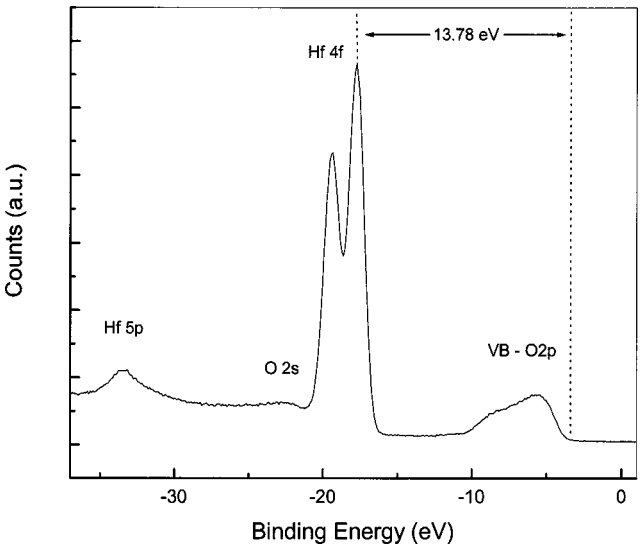

FIG. 1. Soft x-ray photoemission spectra of valence band region for a 28 Å $HfO_2/SiO_xN_y/p$-Si gate stack.

in the vicinity of the Fermi level by a step function and a Gaussian function whose width represents the experimental spectrometer response function. In the case of photoemission experiments, the obtained spectrometer response function is cross checked by the width of the Au 4*f* doublet, which is equal to the combined broadening due to core-hole lifetime and the spectrometer response function. In this case, the core-hole lifetime for the Au $4f_{7/2}$ peak is calculated to be 0.32 eV, in accordance with literature values.[9,10] The spectrometer response functions had Gaussian widths of 0.67 and 0.50 eV for photoemission and inverse photoemission experiments, respectively.

B. XRD measurements

X-ray diffraction studies were performed on a series of films of different thicknesses (Fig. 3). The thickness range

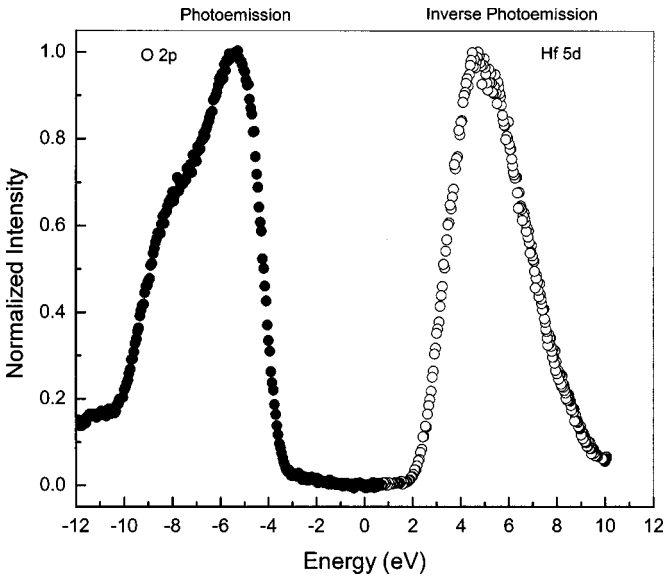

FIG. 2. Combined photoemission (●) and inverse photoemission (○); spectra of a 28 Å $HfO_2/SiO_xN_y/p$-Si gate stack.

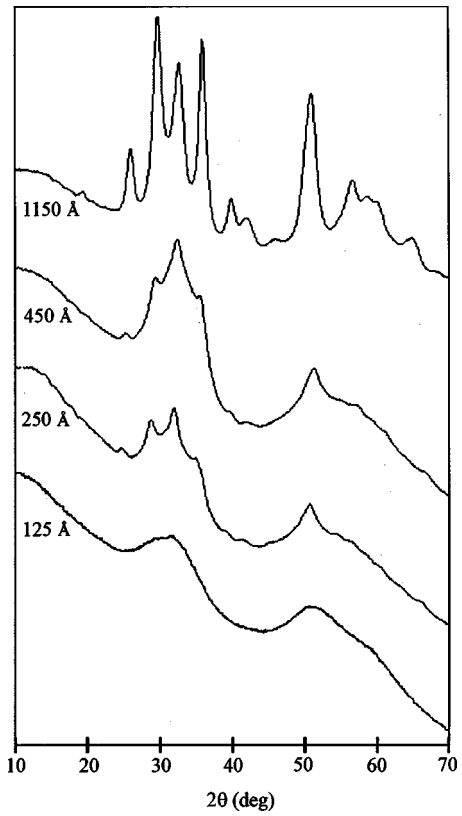

FIG. 3. X-ray diffraction data for four different HfO_2 layer thicknesses: 125, 250, 450, 1150 Å.

was 125–1150 Å, as determined by RBS assuming a density of 9.68 g/cm^3 for all samples. All 12 of the significant diffraction peaks for the 1150 Å sample were consistent with monoclinic HfO_2.[11] As the thickness is reduced, the crystallinity of the films decreases, as is evident from the broadening of the diffraction peaks, consistent with a decrease in the average scattering domain. The diffraction peaks for orthorhombic HfO_2 can be differentiated from those of monoclinic HfO_2 by *d*-spacing comparison alone. The absence of significant diffraction intensity at the *d* spacings of maximum intensity for the orthorhombic phases ($2\theta = 30.4°$ and $32.1°$),[11,12] is strong evidence that the orthorhombic phases are not present to any significant degree. We have also reported Fourier transform infrared studies on these samples, where we identified the presence of the monoclinic phase through an assignment of IR-active phonon modes.[13]

C. Methods for determination of band edges

We (X.Z. and D.V.) have recently performed first principles density functional theory (DFT) calculations on all crystal phases of HfO_2; details of these calculations can be found elsewhere.[3] Although the band gap is not calculated exactly in this method, the shapes and densities of state of the occupied and unoccupied bands are thought to be accurate. Since the crystal structure of these films was determined to be predominantly monoclinic, only the theoretical density of states for monoclinic HfO_2 is considered here. The VBM and CBM as determined from the "raw" DFT band structure of the monoclinic phase calculation yield an energy gap of 3.76 eV. In order to determine a more accurate gap as well as the VBM and CBM positions, we have employed the following procedure which combines experimental and theoretical results. First the theoretical density of states for monoclinic HfO_2 is convoluted with the appropriate spectrometer response functions for both PES and IPES spectra. The height of the first main peak below (above) the VBM (CBM) is normalized (such that the experimental and theoretical heights are the same). Then the broadened theoretical curves in the band edge region are shifted until they align with the experimental curves. The energy shifts needed to align the experimental (PES and IPES) and theoretical densities of states are added to the theoretical gap to obtain a new effective band gap of 6.70 eV. The energy separation ($\Delta E_{CBM} = E_{CBM} - E_f$ and $\Delta E_{VBM} = E_{VBM} - E_f$) between the Fermi level and the VBM and CBM are found to be 3.87 and 2.83 eV, respectively.

If, on the other hand, we were to use the conventional method of linear extrapolation of the experimental valence and conduction band edges to the background intensity level, we would obtain a value of 5.86 eV for the band gap and 3.54 and 2.32 eV for the ΔE_{CBM} and ΔE_{VBM} values, respectively. The difference in these two sets of numbers show that the methodology of VBM and CBM assignment is a greater source of uncertainty in E_{gap} and barrier height determination than the experimental result itself. It is also important to note that photoemission and inverse photoemission give a one particle energy gap that, although wider than the conventionally reported optical gap (which usually involves an exciton), may be more relevant to understanding tunneling through a dielectric. Other methods of gap and edge determination such as UV/Vis spectroscopy, x-ray photoemission spectroscopy (XPS) with shake-up spectral analysis, near-edge x-ray absorption spectroscopy (XAS), should include the exciton gap which may be as high as 1–2 eV in some oxides.

D. Determination of band offsets

Figure 4(a) shows the theoretical density of states of the valence and conduction bands for this system. In Fig. 4(b), the theoretical density of states is convoluted with the instrumental response function, and is plotted along with the experimental measurement of valence and conduction bands. Good agreement is observed between the experimental and theoretical valence band densities of states (specifically the band widths and main features), even though the theoretical density of states is not modified for photoemission cross sections (transition matrix elements). However one would expect that the photoelectron cross section across the band would be similar (if not the same) since the valence band is almost exclusively made up of oxygen 2*p*-like orbitals of σ and π symmetries. In the case of the unoccupied conduction band, the overall width of the band and the first two features agree reasonably well with theory. However the intensity in the higher energy region of the conduction band clearly does not agree well.

In order to extract the valence and conduction band offsets, a knowledge of the position of the Fermi level within the silicon band gap is required. The substrate used was

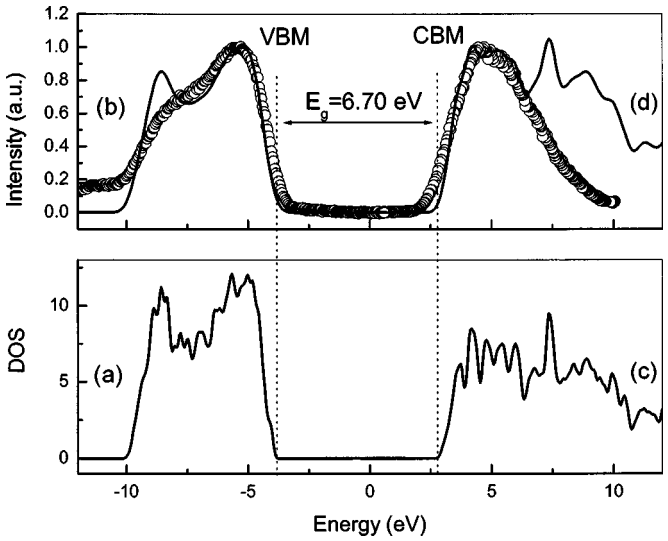

FIG. 4. (a) Theoretical valence band density of states (DOS) for monoclinic HfO_2, (b) photoemission spectra of HfO_2 thin film along with convoluted DOS, (c) theoretical conduction band DOS for monoclinic HfO_2, and (d) inverse photoemission spectra of HfO_2 thin film along with convoluted DOS.

p-type Si with a doping concentration of 1×10^{15} cm^{-3}. The position of the Fermi level with respect to the CBM and VBM of Si can be calculated using standard methods.[14,15] To obtain the (Si-HfO_2) offsets, the energy separation between the Fermi level and CBM of Si is subtracted from the position of the CBM of HfO_2 with respect to the Fermi level (using our combined experimental-theoretical method). Figure 5 shows a simplified energy band diagram for this gate stack. The valence and conduction band offsets are then found to be 3.61 and 1.97 eV. These offsets are large enough to confirm HfO_2 to be a viable high-*k* candidate from a barrier height perspective. However in order to be able to compare the values with results found by others, one must remember to specify the phase of the HfO_2 as well as the method of edge or gap determination. An additional property of the dielectric material, the electron affinity (EA), can also be determined. Since both the electron affinity of silicon (4.15 eV) and the conduction band offset are known, the electron affinity of HfO_2 can be extracted as 2.18 eV (Table I). If the straight-line method is used to determine the offset, we obtained 3.28 and 1.46 eV for the valence and conduction band offsets respectively. Another useful result is that the energy separation between the Hf $4f_{7/2}$ and the VBM are

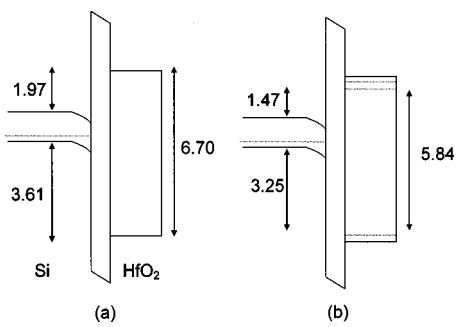

FIG. 5. Simplified energy band diagram of $HfO_2/SiO_xN_y/n$-Si gate stack (a) intrinsic (b) including band-tail states.

TABLE I. The extracted values for band gap E_g, electron affinity EA, conduction band offset CBO, valence band offset VBO, and the energy separation between Hf $4f_{7/2}$ photelectron line and valence band maximum [ΔE (Hf$4f_{7/2}$−VBM)]. Experiment/theory is determined by assuming perfect crystallinity while the effective values are extracted by including the band tail states (at the 2σ level). All values are in units of eV.

Experimental values	Experiment/Theory	Effective values	Straight-line method
E_g	6.70	5.84	5.86
EA	2.18	2.68	2.69
CBO	1.97	1.47	1.46
VBO	3.61	3.25	3.28
ΔE (Hf$4f_{7/2}$−VBM)	13.78	14.14	14.11

determined. The energy separation between a given core level (the $4f_{7/2}$ can be treated essentially as a core here as it is not involved in bonding) and the VBM is constant for a given material; both shift in essentially an equivalent manner as one changes the chemical environment or local field. Thus even in the absence of valence band measurements, by measuring the binding energy of this level, one can easily locate the VBM for a given HfO_2 system. The energy separation between the two is (ΔE Hf $4f_{7/2}$−VBM) is 13.78 eV (see Fig. 1). Experimentally determined values are summarized in Table I.

Figure 6(a) shows PES and IPES spectra of the substrate SiO_xN_y/p-Si, and as well as 10 Å and 28 Å HfO_2 films [Figs. 6(b) and 6(c)]. The substrate silicon yield is visible through the thinner HfO_2 films. The positions of the VBM and CBM are the same as are observed in the thicker film case, hence the band gap is equal to that of the thicker sample. This set of data, along with similar measurements performed on thicker HfO_2 samples, indicate that bulk behavior is reached within the first few (3–4) monolayers of the oxide.

E. Band bending in silicon

The photoemission spectra of the Si 2*p* region before and after deposition, as well as following a forming gas an-

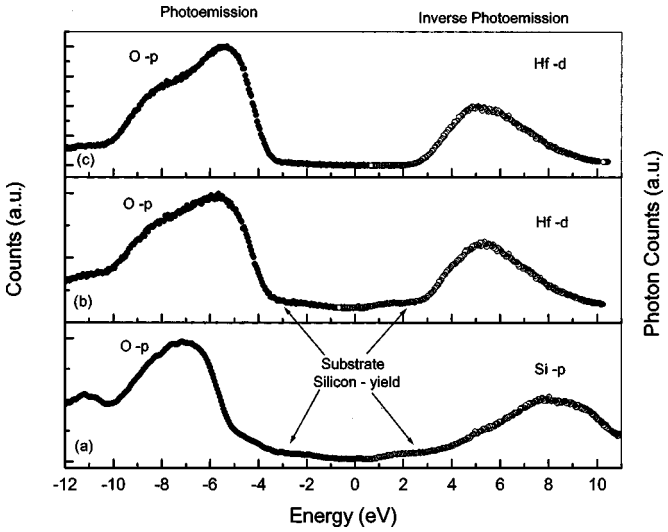

FIG. 6. Combined PES and IPES spectra of (a) 11 Å SiO_xN_y/p-Si, (b) 10 Å $HfO_2/SiO_xN_y/p$-Si, and (c) 28 Å $HfO_2/SiO_xN_y/p$-Si.

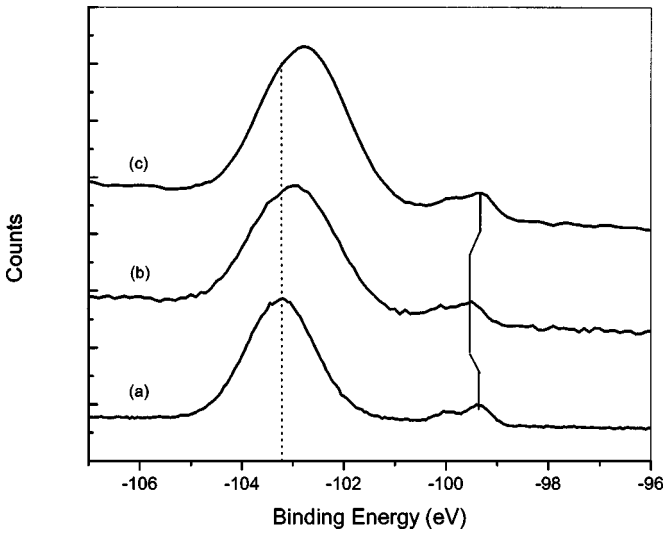

FIG. 7. SXPS spectra of Si 2*p* region of (a) SiO_xN_y/p-Si, (b) as-deposited $HfO_2/SiO_xN_y/p$-Si, and (c) $HfO_2/SiO_xN_y/p$-Si after FGA.

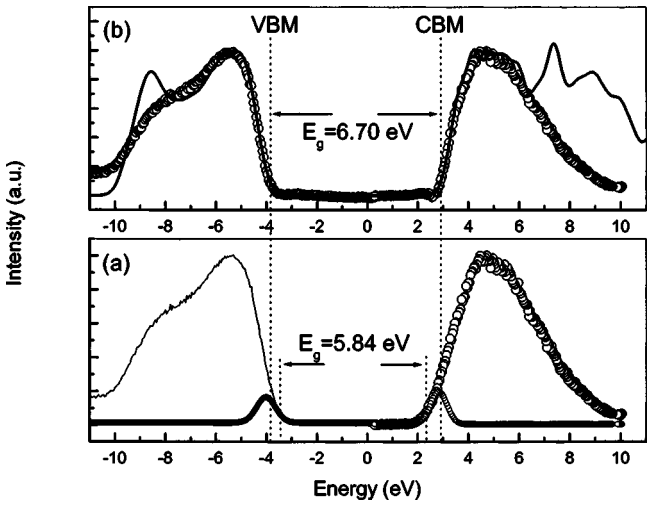

FIG. 8. (a) Densities of states of monoclinic HfO_2 as determined by PES and IPES, the Gaussian peaks roughly model the presence of occupied and unoccupied band-tail/defect states in the vicinity of the VBM and CBM. (b) The fit between theoretical and experimental DOS improves after the band tail states subtracted from the measured DOS.

neal (FGA), are shown in Fig. 7. The binding energy of the Si° $2p_{3/2}$ is measured to be 99.30 eV. There is another band associated with the Si^{+4} species, which is about 3.91 eV away from the Si° $2p_{3/2}$ peak (the curve fitting is not shown, as it is not trivial). A shift in the unoxidized $Si2p_{3/2}$ peak of about 0.26 eV towards higher binding energy is observed after deposition, consistent with band bending. An additional feature around ~3.2 eV on the higher binding energy side of this peak is observed and is tentatively attributed to Si in a $(HfO_2)_x(SiO_2)_y$ silicate, implying a finite level of intermixing at the HfO_2/SiO_2 interface.

F. Comparison of theory and experiment: Band tail states

The theoretical calculations presented in this paper are for bulk oxide crystals of infinite extent. As noted above, due to finite crystallinity of the ultrathin films and the presence of structural and compositional defects, electrical defects may appear. The defects could be charged or neutral, according to their atomic nature, and could in principal exist anywhere (in space and/or energy) in the film. Experimentally, interfacial and/or bulk defect states are observed in a variety of alternative high permittivity materials, some with defect densities on the order of 10^{13} cm^{-2} eV^{-1} (which translates to a bulk density of 10^{19} cm^{-3}). This value is high enough that these states may contribute to the observed photoemission and inverse photoemission yield near the band edges. Because of the observed excess density of states near the band edges and the consequence this has on the band edge definition, two values for the offsets as well as the band gap are noted. One solution would be to simply report an average local density of states at each position across the film, and not to define a gap or pair of edges (as preferred by the device community). One way to understand the defect state energies would be to assume a distribution of defect states in the vicinity of the band edges, as the data suggest. If the experimentally determined DOS is taken and subtracted from the theoretical DOS (following normalization), the difference yields two peaks close to the two band edges. These two peaks can be modeled as a pair of Gaussian curves (Fig. 8) with centrums at −4.01 and 2.83 eV, and widths of 0.58 and 0.59 eV (after subtracting out the corresponding spectrometer response functions outlined above). The literature consensus is that HfO_2 films have a gap of 5.6–6.0 eV, although the proof and methodology of this remains debated.[16–20] We obtain this value from our results by defining the edge as the 2σ level of the Gaussian-modeled band tail states. Although there is no strong theoretical argument to include what we are calling band edge defect states in defining the "real" gap, they may be considered as contributing to an "effective" band gap (see Fig. 8). We also include these effective values in Fig. 5.

Concerning their physical nature, one of the conventional assignments of the observed defect states would be to attribute them to band-tail states. The presence of structural disorder can also be caused by (or related to) deviations from ideal stoichiometry (metal vacancies, excess oxygen, oxygen vacancies or impurities such as atomic hydrogen). In fact, these films do contain slightly higher oxygen content than the ideal stoichiometry (at least as measured by MEIS following growth) and are also likely to contain excess hydrogen as deposited. Peacock and Robertson have shown that atomic hydrogen, as an extrinsic defect, would introduce shallow unoccupied states in the vicinity of the conduction band which behave as acceptors.[21] Foster *et al.* reported on the vacancy and interstitial defects in HfO_2 where it is theoretically shown that the O_2^- species would introduce defect states in the vicinity of the valence band. These states are neutral when occupied, and act as donors.[22]

Kerber *et al.* reported on conventional charge pumping results on a $HfO_2/SiO_2/Si$ dual-layer gate stack.[23] The charge measured with an amplitude sweep, along with the observation of a strong dependence on charging/decharging time, supported the proposition that defects were located deeper inside the gate stack. All the observed features in the experimental data could be explained qualitatively if defects

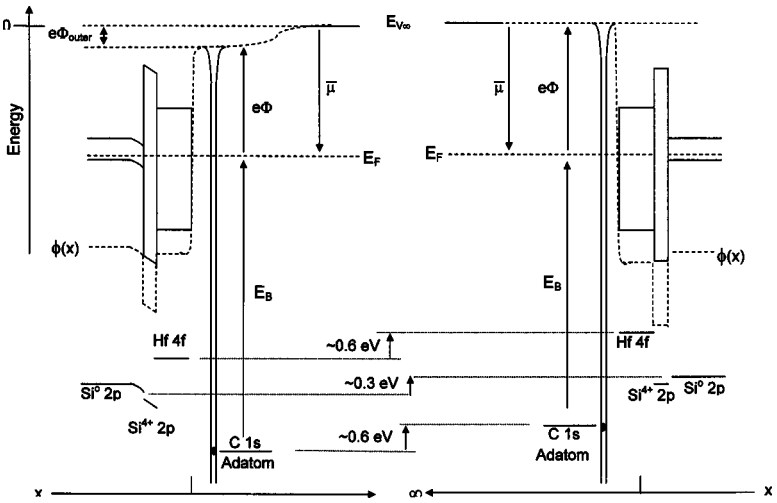

FIG. 9. The electrostatic potential distribution across gate stack (a) as-deposited (b) after a forming gas anneal at 400 °C.

were located in a HfO_2 layer distributed in energy and space. It was also argued that the defect states are above the silicon conduction band minimum whose origin was attributed to oxygen vacancies and/or impurities in HfO_2. The energy of the states observed in our work (in the vicinity of the HfO_2 conduction band minimum) is qualitatively consistent with those proposed by Kerber *et al.*

G. Electrostatic potential across the gate stack

The charge neutrality level (CNL) of semiconductor surface (interface) states is defined as the energy above which the states are empty for a neutral surface (interface).[11] The band alignment between two semiconductors is believed to be controlled in part by charge transfer across the interface which results in the creation of interface dipoles. This dipole modifies the barrier heights given by the electron affinity rule,[24] which is basically the difference between the electronegativities screened by a factor which depends on the electronic component of the dielectric constant. In the case of HfO_2, the bulk CNL lies above the Fermi level of the *p*-doped silicon substrate (in other words the electronegativity of HfO_2 is smaller than that of the silicon substrate).[18] An equalization of the electrochemical potentials occurs when the materials are brought into contact which creates a dipole at the interface. This interface dipole alters the occupancy of interface states due to the charge transfer from HfO_2 to silicon. This leaves positive charge on the dielectric side of interface, with opposite charge appearing in silicon to screen it. This is consistent with our finding of downwards band bending observed for substrate silicon since the downward bending for a *p*-type silicon substrate is indicative of the presence of negative charge in the silicon. Furthermore the amount of charge can be calculated from the observed band bending in silicon by plotting the surface potential versus charge curve. The amount of charge, for a band bending of 0.26 eV, is found to be 6×10^{12} cm^{-2}, which is in good agreement with the electrical measurements.[23]

The energy of the orbitals that carry this positive charge (that is compensated for by a buildup of negative charge in silicon substrate) is of concern. Due to the presence of charges within the gate stack, electrostatic potentials are developed across it. One scenario is depicted in Fig. 9. The electrostatic potential just outside the surface will be either positive or negative with respect to the potential at infinity, depending on the whether the material's electrochemical μ_e potential is smaller or larger than the local work function ϕ.[25] In Fig. 9, this is illustrated for a smaller local work function. If one can devise a method to probe this potential just outside the surface, then information regarding local work function will be reached. One such tool is to take advantage of surface hydrocarbons due to atmospheric contamination; this is similar to putting inert adatoms (such as Kr, Xe, etc.) on the surface.[26,27] Although the hydrocarbon species become bound to the surface, they are usually only physisorbed, hence their electronic states are pinned to the local vacuum level (not the Fermi level). One should be careful when analyzing such charging, as local fields and polarization can shift the relevant states. In our studies, we used thin dielectric films (no thicker than 30 Å) and checked for charging as function of flux and time; no indication of charging is found within the experimental resolution. Our energy reference is the Fermi level obtained by analyzing the valence band region of clean polycrystalline inert metal foils (Au, Pt, Ag, etc.). The Fermi energy observed in this manner can be used to determine the spectrometer work function. To convert the measured kinetic energies to binding energy, the spectrometer work function should be subtracted from the difference between the excitation energy and the kinetic energy. In this way, the measured binding energies would all be referenced to the same Fermi level. As shown in Fig. 10, the binding energies of the C 1*s* photoelectron peak from surface hydrocarbons on a Au or Pt surface differ by about ~0.5 eV which corresponds to the work function difference between Au and Pt (the latter being larger). The *p*-Si used as substrate has a doping level of 1×10^{15} cm^{-3} which places the Fermi level at 0.26 eV above the valence band. Using this information together with the electron affinity of silicon, one obtains a work function of ~5.0 eV for this particular substrate, which is very close to the work function of gold. However, the C 1*s* position differs from that of Au by about ~0.6 eV. This indicates a local work function change of ~0.6 eV. Following a forming gas anneal, the C 1*s* positions for both the sample and gold align perfectly, indicating the expected result of equal work functions (~5.0 eV). Following a form-

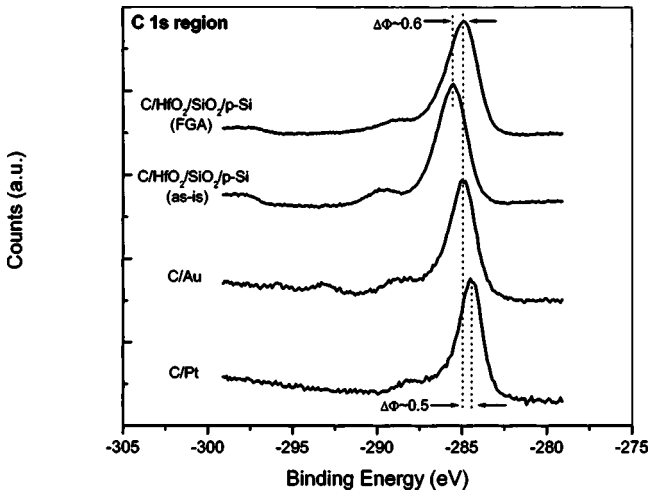

FIG. 10. XPS spectra of the C 1*s* region of surface hydrocarbon contamination on substrates of different work functions.

ing gas anneal (which is known to reduce the number of defects in the gate stack), the Si 2*p* levels shift by about ~0.26 eV whereas the Hf 4*f* and C 1*s* levels shift by ~0.55 eV. Since any photoelectron originating from layers above the charge should shift in equal amounts, this leads us to infer that the positive charge is located primarily close to the SiO_2/HfO_2 interface. This observed shift is due to the electrostatic potential across the gate stack, hence the energy band diagram should be corrected for this potential.

IV. CONCLUSION

We have studied the $HfO_2/SiO_xN_y/p$-Si gate stack by PES and IPES along with first principles calculations. The HfO_2 films experimentally examined were predominantly monoclinic. Combined experimental and theoretical calculations were used to locate the valence band maximum and conduction band minimum. The method used takes into account the spectrometer response function, hence the broadening of the spectral features due to limited resolution by excitation source, electronics, etc.

Evidence for the presence of charge in the gate stack is presented, along with a discussion of possible structural and/or compositional origins for the charge defects. The electron affinity of monoclinic HfO_2 is calculated to be 2.18 eV from the measured band offset and the known electron affinity of silicon. The energy separation between the Hf $4f_{7/2}$ core level and the VBM is measured and found be 13.85 eV. This energy difference can serve as a valuable input for photoemission studies on this material since measuring the binding energy of this core level will enable one to locate the VBM.

Although the presence of defects on spectroscopic and electrical behavior are observed, the origin of the defects could not be unambiguously understood with the presently available data and theory. The presence of band-tail states, as revealed by the comparison of theoretical and experimental results may originate from disorder in the film.

ACKNOWLEDGMENTS

The authors would like to thank the SRC, Sematech, and the NSF for financial support. We also thank J. Robertson, S. Chambers, R. Opila, E. Gusev, T. Gustafsson, and G. Wilk for useful discussions. D. Vanderbilt and X. Zhao acknowledge NSF Grant No. DMR-0233925 for financial support.

[1]International Technology Roadmap for Semiconductors, Semiconductor Industry Association (2003).
[2]G. D. Wilk, R. M. Wallace, and J. M. Anthony, Appl. Phys. Rev. 89, (2001).
[3]X. Zhao and D. Vanderbilt, Phys. Rev. B **65**, 075105 (2002).
[4]X. Zhao and D. Vanderbilt, Mater. Res. Soc. Symp. Proc. **747**, 93 (2003).
[5]D. Redfield, J. P. Wittke, and J. I. Pankove, Phys. Rev. B **2**, 1830 (1970).
[6]C. H. Olk and S. M. Yalisove, Phys. Rev. B **52**, 1692 (1995).
[7]P. Y. Yu and M. Cardona, in *Fundamentals of Semiconductors*, 3rd ed. (Springer, Berlin, 2001), pp. 159–202.
[8]S. Sayan, S. Aravamudhan, B. W. Busch, W. H. Schulte, F. Cosandey, G. D. Wilk, T. Gustafsson, and E. Garfunkel, J. Vac. Sci. Technol. A **20**, 507 (2002).
[9]P. H. Citrin and G. K. Wertheim, Phys. Rev. Lett. **41**, 1425 (1978).
[10]E. A. Kraut, R. W. Grant, J. R. Waldrop, and S. P. Kowalczyk, Phys. Rev. B **28**, 1965 (1983).
[11]R. E. Hann, P. R. Suitch, and J. L. Pentecost, J. Am. Ceram. Soc. **68**, C285 (1985).
[12]O. Ohtaka, T. Yamanaka, and S. Kume, J. Ceram. Soc. Jpn. **99**, 826 (1991).
[13]M. M. Frank, S. Sayan, S. Dörmann, T. J. Emge, L. S. Wielunski, E. Garfunkel, and Y. J. Chabal, Mater. Sci. Eng., B **109**, 6 (2004).
[14]S. M. Sze, *Physics of Semiconductor Devices*, 2nd ed. (Wiley, New York, 1981).
[15]K. Kano, *Semiconductor Devices* (Prentice-Hall, Upper Saddle River, NJ, 1998).
[16]V. V. Afanas'ev, A. Stesmans, F. Chen, X. Shi, and S. A. Campbell, Appl. Phys. Lett. **81**, 1053 (2002).
[17]A. Callegari, E. Cartier, M. Gribelyuk, H. F. Okorn-Schmidt, and T. Zabel, J. Appl. Phys. **90**, 6466 (2001).
[18]J. Robertson, J. Vac. Sci. Technol. B **18**, 1785 (2000).
[19]J. Robertson, Appl. Surf. Sci. **190**, 2 (2002).
[20]M. Balog, M. Schieber, M. Michman, and S. Patai, Thin Solid Films **41**, 247 (1977).
[21]P. W. Peacock and J. Robertson, Appl. Phys. Lett. **83**, 2025 (2003).
[22]A. S. Foster, F. L. Gejo, A. L. Shluger, and R. M. Nieminen, Phys. Rev. B **65**, 174117 (2002).
[23]A. Kerber *et al.*, IEEE Electron Device Lett. **24**, 87 (2003).
[24]R. L. Anderson, Solid-State Electron. **5**, 341 (1962).
[25]W. F. J. Egelhoff, Surf. Sci. Rep. **6**, 213 (1986).
[26]T. V. W. Janssens, G. R. Castro, and K. Wandelt, Surf. Sci. **399**, 15 (1998).
[27]T. V. W. Janssens, G. R. Castro, K. Wandelt, and J. W. Niemantsverdriet, Phys. Rev. B **49**, 14599 (1994).
[28]S. Sayan, R. A. Bartynski, X. Zhao, E. P. Gusev, D. Vanderbilt M. Croft M. Banaszak-Holl and E. Garfunkel, Phys. Status Solidi B **241**, 2246 (2004).